The 9th European Congress on Computational Methods in Applied Sciences and Engineering
ECCOMAS Congress 2024
3–7 June 2024, Lisboa, Portugal

TOPOLOGY OPTIMIZATION OF SUPPORT STRUCTURES FOR 3D PRINTING USING LENGTH CONTROL AND ADDITIVE MANUFACTURING GUIDELINES ECCOMAS CONGRESS 2024

JOAQUÍN CASTRO[1*], EDUARDO FERNÁNDEZ[1], PIERRE DUYSINX[1], PAULO FLORES[2] AND CARLOS MEDINA[2]

[1] Aerospace and Mechanical Engineering Department
University of Liege
Allée de la Découverte 9, 4000 Liège, Belgium
*e-mail: jcastro@uliege.be

[2] Mechanical engineering department
Universidad de Concepción
Edmundo Larenas 219, Concepción, Chile

Key words: Topology optimization, Additive manufacturing, Supports structures, Length control

Summary. This work uses Topology Optimization (TO) as a design tool for the generation of support structures for Additive Manufacturing (AM). The compliance minimization problem subject to a volume constraint is considered as optimization criteria. To ensure the mechanical functionality of the optimized supports, the geometrical guidelines of a 3D printer are empirically identified and introduced as design constraints in the TO problem using length scale control. The propose methodology is implemented in a density-based TO formulation and validated on 2D benchmarks, which are subsequently extruded and fabricated using an Ultimaker S2$^+$ 3D printer.

1 INTRODUCTION

Additive manufacturing has experienced incredible growth in the industry due to its ability to fabricate components with complex geometries, which allows for improved design performance compared to those intended for conventional manufacturing processes [1, 2, 3]. Despite the design freedom provided by the layer-by-layer approach, AM faces limitations with certain geometrical features. Most notably, the difficulty of depositing material in overhang areas that do not have sufficient support may affect surface quality, geometric accuracy, or cause the component to collapse during manufacturing [4].

Various approaches have been developed to address the limitations associated with unsupported geometrical features in AM. One approach involves optimizing the orientation of the part to minimize or eliminate critical overhang angles of down-facing surfaces [5, 6]. Similarly, the design of the component can be modified so the critical overhang angle of design features is reduced, either manually or using shape optimizers [7]. When the design is still in the conceptual phase, overhang angle constraints can be integrated into the design process. For instance,

applying this criterion in TO ensures the successful printing of the component [8]. However, if the design is already conceived and cannot be modified, and if the 3D printer is equipped with a fixed printing direction that cannot be rotated, then supporting structures are required to provide mechanical support. These structures may also be required as heat extractors [9] or stiffeners to avoid thermo-mechanical distortions [10, 11]. Nevertheless, these support structures demand more material and printing times, which increase the manufacturing cost. Additionally, since support structures are only needed during the printing process, they become waste once printing is completed and require extra effort and tooling for removal.

Due to the shortcomings associated with the use of support structures, significant efforts have been dedicated to reducing the material usage, printing time, and energy required for their removal. Some methods have explored the use of cellular structures [12], lattice support structures [13], honeycomb supports [14], and tree-like supports [15, 16], among others. These methods predominantly employ predefined geometric patterns to optimize support structure designs. An alternative approach is the use of TO as a design tool to generate these support structures. This method is capable of generating complex and high-performance designs without a preconceived geometric pattern [17]. For instance, [18, 19, 20] generated support structures using TO, aiming at improving heat dissipation, which is an important criterion in metal AM processes. Kuo et al. [21] aimed at generating support structures with TO by employing a repulsion index to minimize contact areas, thus facilitating easier removal of support structures [10]. Langelaar [22] considered the optimal design of the component, support structures, and printing orientation.

It is noteworthy that most of the cited works are limited to reporting their designs without 3D printing the AM component and its support structures, thereby restricting a detailed analysis of the proposed methods' scope and limitations. In the work of Mezzadri et al. [23] an experimental validation of support structures generated with TO was included. They incorporated minimum size constraints in the TO formulation and conducted a parametric study on optimization parameters such as volume fraction, boundary conditions, and domain aspect ratio, among others. The printed support structures were more efficient compared to those generated by Ultimaker's Cura software [24]. However, their TO-based supports had large contact areas, which could complicate the post-removal process of the support structures.

Our work presents a novel strategy for designing support structures using TO. This approach involves identifying a set of geometric guidelines specific to a given 3D printer and incorporating them as constraints in the TO problem. Specifically, we employ a TO formulation capable of controlling the minimum member size, minimum cavity size, maximum member size, and minimum distance between members [25]. Additionally, we introduce two new strategies to control the distance of the contact points between the supports and the AM component: one based on minimum gap constraints and the other by modifying the boundary conditions of the finite element model. The strategies are tested using different 2D benchmarks, which are extruded and fabricated using an Ultimaker S2$^+$ 3D printer.

This paper is organized as follows: Section 2 presents the formulation of the TO problem adopted in this work. Section 3 gathers the geometric guidelines for the Ultimaker S2$^+$ printer. Section 4 presents the influence of including the collected geometric guidelines in the generation of support structures using TO. Section 5 provides a set of TO-based designs for benchmark problems and the corresponding 3D-printed supports. Finally, the conclusions of this work are detailed in Section 6.

2 TOPOLOGY OPTIMIZATION FRAMEWORK

This work assumes that the part to be printed cannot be rotated with respect to the baseplate and its geometry cannot be modified, so the design procedure is focused only on the supporting structures. For this purpose, a density-based TO approach is employed. In this approach, the design domain of the supporting structures is discretized into N finite elements, and each finite element is associated with a pseudo density $\bar{\rho}$, which ranges between 0 and 1 to represent the absence and presence of material, respectively. The mechanical contribution of each finite element i to the whole support structure is controlled by its Young's modulus E_i, which is computed using the SIMP (Solid Isotropic Method with Penalization) approach as follows:

$$E_i = E_{\min} + \bar{\rho}_i^{\eta}(E_0 - E_{\min}) \ , \quad i = 1, \ \dots \ , N \ , \tag{1}$$

where E_0 and $E_{\min}$ represent the Young's modulus of the base material and of the phase representing the absence of material, respectively. In practice, $E_{\min}$ is chosen as a very small value to prevent significant mechanical contribution while avoiding numerical singularities in the finite element analysis.

The finite element model that assesses the performance of the supporting structures is illustrated in Figure 1. The AM part to be printed is shown in yellow, and the design space where supporting structures are needed is shown in gray. To simplify the model, it is assumed that the force imposed by the layer deposition on the support structures is due only to the part weight, that the load distribution is not influenced by the design of the supporting structures, and that the force acts in the opposite direction to the printing direction, as illustrated in Figure 1. Given the focus of this study on ensuring successful printing through geometric considerations, thermomechanical effects such as large thermal gradients that induce material anisotropy, mechanical distortions, and other complex and computationally expensive multiphysics phenomena are omitted.

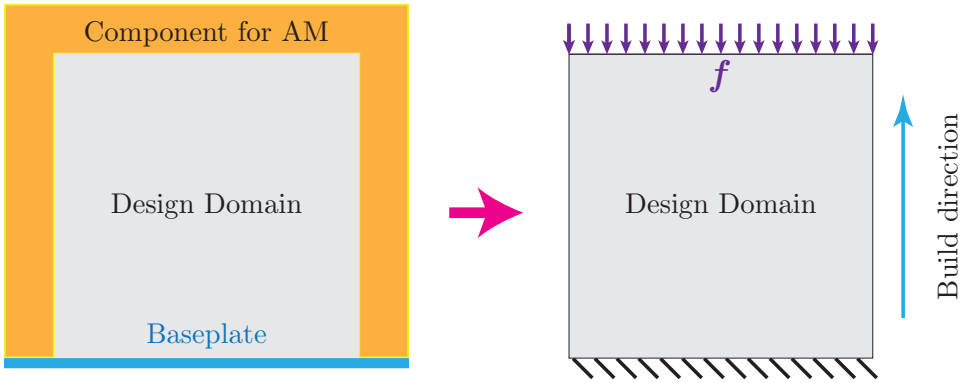

Figure 1: On the left, the part to be printed and the domain where supporting structures are needed. On the right, the design domain of supporting structures and boundary conditions used for TO.

The geometry of the support structures is optimized to maximize the stiffness of the supports subject to a mass constraint. In addition, minimum and maximum member size and minimum cavity size control are included in the TO problem in order to impose geometrical features over

the design based on geometric guidelines that ensure successful 3D printing. For this purpose, the adopted TO problem is as follows:

$$\begin{aligned} \min_{\rho} \quad & \mathbf{f}^{\intercal}\,\mathbf{u} \\ \text{s.t.:} \quad & \mathbf{K}(\bar{\boldsymbol{\rho}})\,\mathbf{u} = \mathbf{f} \\ & \mathbf{v}^{\intercal}\bar{\boldsymbol{\rho}} \leq V^{*} \\ & G_{\text{ms}}(\bar{\boldsymbol{\rho}}) \leq 0 \\ & G_{\text{mg}}(\bar{\boldsymbol{\rho}}) \leq 0 \\ & 0 \leq \rho_i \leq 1 \ , \ i = 1 \ , \ \ldots N \ , \end{aligned} \tag{2}$$

where $\mathbf{f}$ and $\mathbf{u}$ are vectors containing the nodal forces imposed by the layer deposition on the supporting structure and the nodal displacements, respectively. $\mathbf{K}$ is the stiffness matrix that assembles the elementary stiffnesses that depend on Young's modulus $E(\bar{\rho})$. V^{*} is the upper bound of the volume constraint, $G_{\text{ms}}(\bar{\boldsymbol{\rho}})$ and $G_{\text{mg}}(\bar{\boldsymbol{\rho}})$ are the maximum size and minimum gap constraints, respectively, and finally, ρ_i is the design variable associated with the finite element i.

The design variables ρ pass through a filtering and projection process. Filtering allows for the avoidance of numerical instabilities that are inherent of the density method [26], while the projection process allows to reduce the number of intermediate densities and impose a precise control over the minimum size of solid members and cavities [27]. Specifically, this work considers the density filter proposed by [28] and the robust formulation that projects eroded, intermediate, and dilated designs [29], as illustrated in Figure 2. It has been demonstrated that the robust formulation that optimizes the material distribution for the worst-performing design, which for the compliance minimization case turns out to be the eroded one, guarantees a minimum size in the intermediate design [27]. In addition, maximum size and minimum gap control can be imposed if the G_{ms} and G_{mg} constraints are imposed at least in the dilated design [25]. The TO problem, including the eroded, intermediate, and dilated fields for effective geometric size control, is as follows:

$$\begin{aligned} \min_{\rho} \quad & \mathbf{f}^{\intercal}\,\mathbf{u} \\ \text{s.t.:} \quad & \mathbf{K}(\bar{\boldsymbol{\rho}}^{\text{ero}})\,\mathbf{u} = \mathbf{f} \\ & \mathbf{v}^{\intercal}\bar{\boldsymbol{\rho}}^{\text{dil}} \leq V^{*} \\ & G_{\text{ms}}(\bar{\boldsymbol{\rho}}^{\text{dil}}) \leq 0 \\ & G_{\text{mg}}(\bar{\boldsymbol{\rho}}^{\text{dil}}) \leq 0 \\ & 0 \leq \rho_i \leq 1 \ , \ i = 1 \ , \ \ldots N \ , \end{aligned} \tag{3}$$

where the superindices ero and dil refer to the eroded and dilated projections, respectively. The designs reported in this work correspond to the intermediate projections, denoted by $\bar{\boldsymbol{\rho}}^{\text{int}}$, as illustrated in Figure 2.

To avoid overextending the description of the TO problem, implementation details are omitted. We refer interested readers to the work of [27] for details about the filtering and projection processes leading to the eroded, intermediate, and dilated designs. For implementation details regarding the maximum size and minimum gap constraints, the reader is referred to the work of [25].

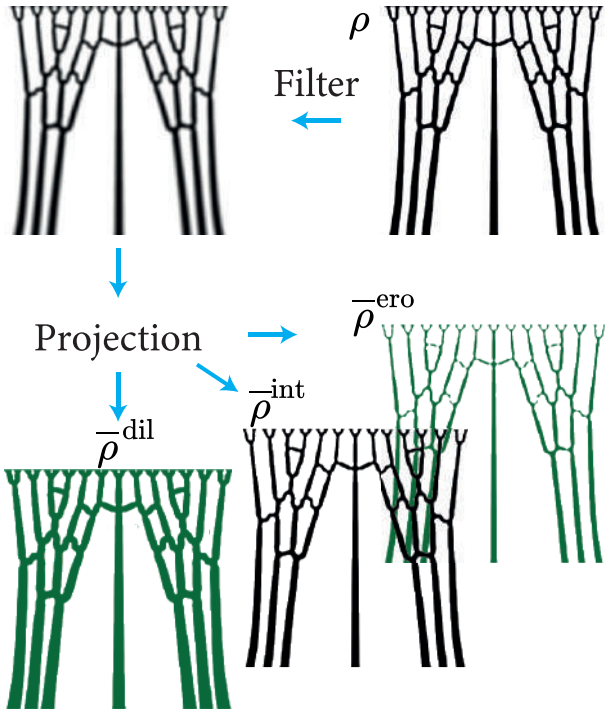

Figure 2: Illustration of the filtering and projection processes used to obtain the eroded, intermediate, and dilated fields.

3 GEOMETRIC AM GUIDELINES FOR SUPPORT STRUCTURES

Table 1: Printer parameters and specifications of the Ultimaker S2$^+$.

Parameters	Values
Layer thickness	0.1 [mm]
Infill density	20%
Infill pattern	Grid
Print speed	20 [mm/s]
Nozzle temperature	210 C^o
Fan speed	100%
Baseplate temperature	60 C^o
Material (Brand)	PLA (Cicla 3D)
Nozzle diameter	0.4 [mm]

To ensure the successful printing and easy removal of TO-generated supports, this study incorporates a set of geometric guidelines specific to a 3D printer into the TO problem equipped with size constraints. It is known that the geometric guidelines depend on the 3D printer, the material, and the printing parameters used [30, 31, 32]. However, since this work focuses on presenting a methodology based on TO, we use a single PLA 3D printer and one set of printing parameters. Specifically, we utilize an Ultimaker S2$^+$ 3D printer and the parameters listed in

Table 1.

To obtain the geometric guidelines, a set of geometric shapes is printed, and the values for which the printing is not successful are detected. The guidelines are selected taking into account 2D designs of support structures, which are extruded in 5 [mm] for 3D printing. These guidelines aim to ensure the supports can be effectively printed and provide adequate structural integrity for both themselves and the parts being printed, while also guaranteeing satisfactory surface quality. The compiled guidelines are summarized in Table 2 and are detailed below.

1. **Minimum wall thickness:** This guideline provides insight into the resolution limitations of the 3D printer. As shown in Figure 3a, a set of thin walls is printed to determine the smallest dimension that can be successfully built. The measured minimum wall thickness is 0.5 [mm].

2. **Minimum hole diameter:** This guideline identifies the diameter of the smallest printable hole, which corresponds to a diameter of 0.8 [mm], as shown in Figure 3b. Smaller holes are closed, so they are excluded from the screening criteria.

3. **Minimum separation between walls:** As shown in Figure 3c, if two walls are spaced less than 0.4 [mm] from each other, they could stick together during the printing process. In the case of support structures, these could stick to the AM component and complicate the removal process.

4. **Maximum aspect ratio:** Given that supporting structures are usually slender when they join the baseplate with the top of the part, a buckling criterion must be considered in order to ensure their printability. To simplify the analysis, the largest aspect ratio (height/width) that can be printed accurately is detected. As shown in Figure 3d, the two thinnest columns were printed, but with large horizontal displacements during the deposition process, which affects the structural stability of the support. For this reason, the highest aspect ratio is obtained from the third thinnest column of Figure 3d, since it showed no evident signs of instability during printing.

5. **Maximum bridge length:** This guideline specifies the maximum distance that a layer can be spread between two supports. The criterion may be to avoid layer collapse or to achieve a specific surface quality. As in the work of [16], it is found that a distance of 2.0 [mm] is suitable for good surface quality, as shown in Figure 4.

Some works [16, 15] have identified an optimal length-to-overhang angle ratio for supports to prevent collapse or excessive displacement during the printing process. This geometric guideline is particularly valuable in support structure design using geometric-based methods, where the structural branch pattern is predetermined. However, based on our experience, it is not essential to impose additional constraints on the TO problem since the vertical stiffness criterion promotes the generation of tree structures with upward-oriented branches, so that overhang angles do not present major challenges when printing the TO-based supports.

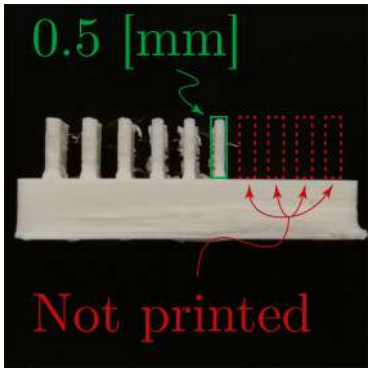

(a) Minimum wall thickness

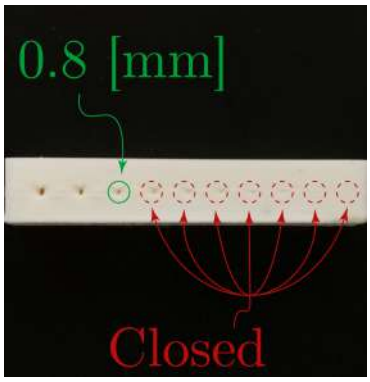

(b) Minimum hole diameter

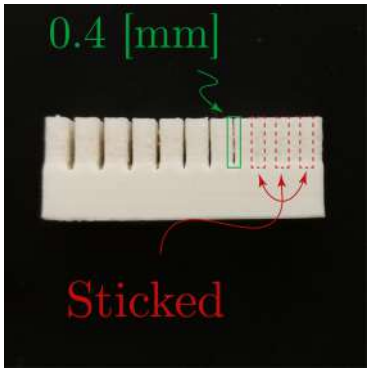

(c) Minimum separation between walls

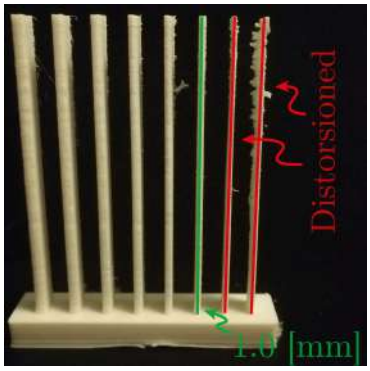

(d) Maximum aspect ratio

Figure 3: 3D-printed geometric patterns to determine the size to impose on the TO problem.

It is important to note that the values obtained for the geometric guidelines were selected qualitatively using non-standardized criteria. Therefore, other users may choose different values according to their needs and quality standards. There are also several other geometric patterns that can serve as a basic guide in the design of supporting structures [33, 34]. Nonetheless, the five patterns listed above have proven to be highly effective for achieving topologically optimized, printable support structures.

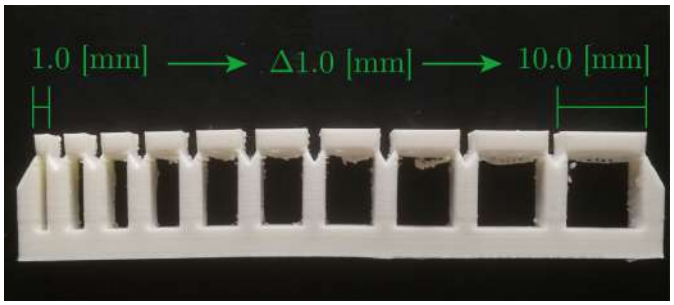

Figure 4: 3D-printed component to obtain the maximum bridge distance to be imposed in TO.

4 TOPOLOGY OPTIMIZATION TAILORED TO GEOMETRIC GUIDELINES

This section discusses the relevance of the collected geometric guidelines in the design of support structures. For this purpose, we consider the 2D domain shown in Figure 1. The size of the design domain is 50 [mm] each side, and it is discretized using 250.000 quadrilateral finite elements. Figure 5 shows the reference solution obtained only with minimum member size control, which is imposed according to the minimum wall thickness (0.5 [mm]). The design exhibits similarities to those reported by Mezzadri et al. [23], yet it demonstrates several drawbacks:

i. It is in contact with the vertical walls of the component at the bottom and top of the design. This could complicate the support removal or affect the surface quality of the component.

ii. It has structural members with a high aspect ratio, such as the central column. This could hinder the fabrication of the column and compromise the structural stability of the upper zone of the supports.

iii. It has large contact areas with the baseplate and the surface of the component, which could complicate support removal and compromise the surface quality of the component.

Table 2: Geometric guidelines for the length control of supports structures generated with TO for the 3D printer Ultimaker S2$^+$.

Geometric guideline	Value
Minimum wall thickness	0.5 [mm]
Minimum hole diameter	0.8 [mm]
Minimum separation between walls	0.4 [mm]
Maximum aspect ratio (Height/Width)	50

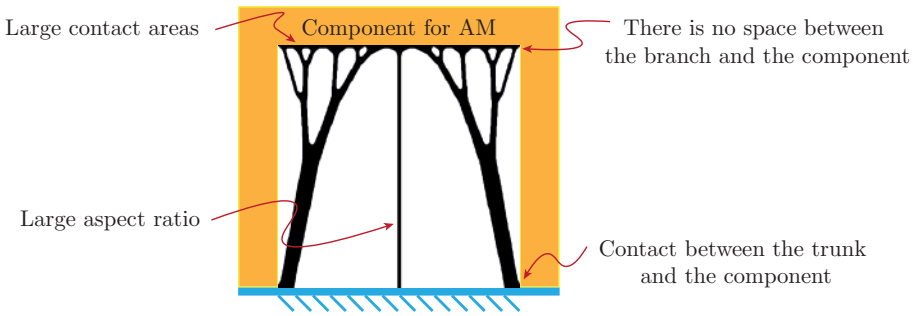

Figure 5: Some design problems of support structures generated with TO when only the minimum wall thickness is considered.

4.1 Distance between support and AM component

The first problem (i) can be avoided by simply reducing the area where the distributed force acts. The objective is to move the trunk and structural branches away from the edges, taking

into consideration the maximum bridging distance and the minimum distance between walls. For example, by imposing a space between the side wall and the force application zone, as shown in Figure 6a, the bonding of the supports with intricate areas such as the corners of the component can be avoided. To ensure good 3D printing, the space between branches and the component cannot exceed the maximum bridging distance (2.0 [mm]). At the same time, a space can be imposed between the fixed degrees of freedom of the supports and the component. This avoid the bonding of the structural trunk with the component wall, therefore, the space between the trunk and the component must be at least equal to the minimum distance between walls (0.4 [mm]). The design obtained with these two local modifications is shown in Figure 6b.

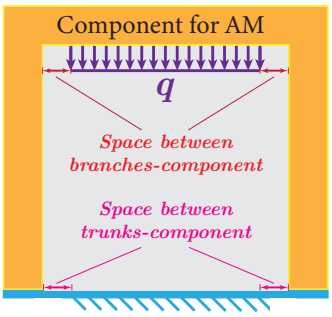

(a) Local modification of boundary conditions.

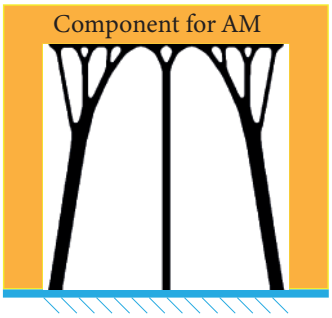

(b) Optimized supports.

Figure 6: Boundary treatment to avoid sticking of the supports to the AM component.

4.2 Aspect ratio control

To address problem (ii) and prevent large aspect ratios, a minimum size requirement is imposed on solid members based on the maximum aspect ratio criterion. For instance, given the design domain height of 50 mm, column thickness should be at least 1 mm to meet the maximum aspect ratio of 50. Within the design domain, the minimum size is imposed as a function of the distance from the layer to the baseplate. For example, considering a linear interpolation, the minimum size imposed in the TO problem is:

$$d_{\min}(y) = \frac{t_{\min}}{y_{\max} - y_0}(y - y_0) - \frac{y - y_0}{R_{\max}} + \frac{y_{\max} - y_0}{R_{\max}} \tag{4}$$

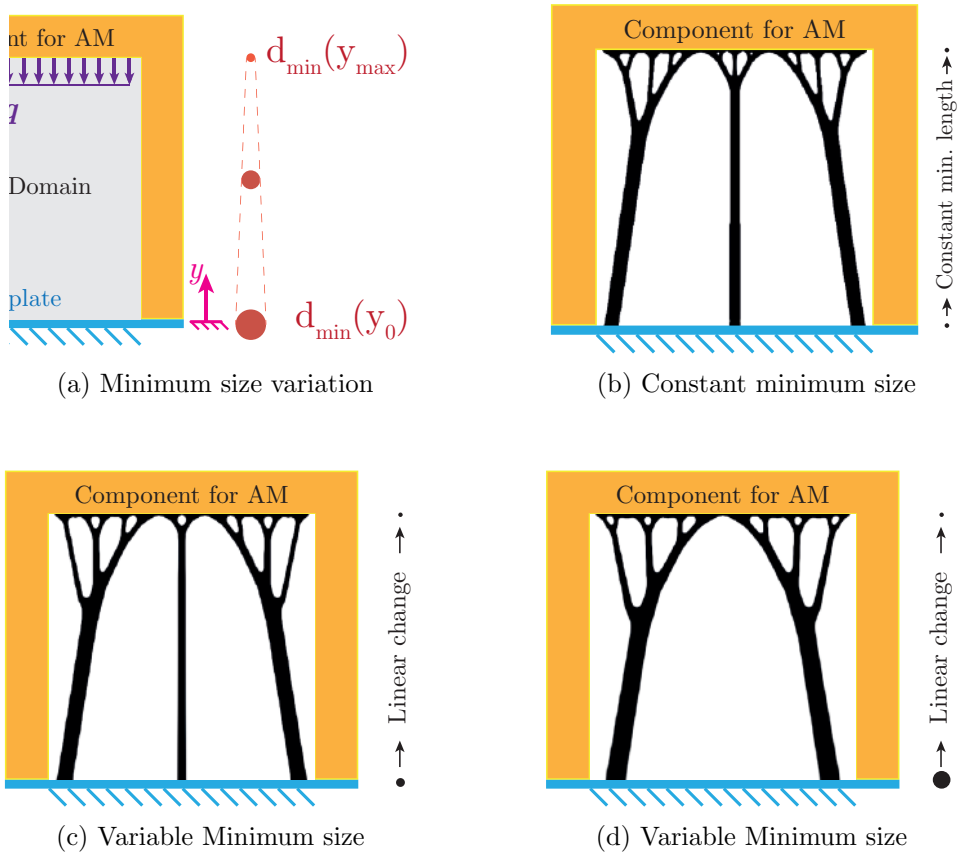

(a) Minimum size variation

(b) Constant minimum size

(c) Variable Minimum size

(d) Variable Minimum size

Figure 7: In a)the scheme showing the variable minimum size of the solid phase. In b) the design obtained with a constant minimum member size. In c) the obtained design with variable minimum member size and maximum aspect ratio 50, and d) with maximum aspect ratio 25.

where $d_{\min}$ is the minimum size imposed in TO. As illustrated in Figure 7a, y is the vertical coordinate, and y_0 and $y_{\max}$ are coordinates of the baseplate and maximum height of the design domain, respectively. $R_{\max}$ is the maximum aspect ratio, which is equal to 50 in this work, and $t_{\min}$ is the minimum wall thickness, equal to 0.5 in this work. Figure 7b shows a design obtained using a constant minimum size equal to $t_{\min}$, while Figures 7c and 7d define the minimum member size as in Eq. (4), using $R_{\max} = 50$ and $R_{\max} = 25$, respectively. Comparing Figures 7c and 7d, it is observed that the maximum aspect ratio condition is effective in avoiding thin columns that cause difficulties during 3D printing.

4.3 Reduction of contact areas

To reduce the area of the contact points (problem iii), a maximum size constraint is applied. Similar to the minimum size constraint discussed earlier, this constraint is linearly adjusted relative to the height from the baseplate to maintain compatibility with the aspect ratio constraint and to minimize contact area. Figure 8 shows how the support structures vary as the thickness increases at the base, but the difference between the minimum and maximum thickness is

maintained. One detail that can be observed is that while all the supports shown in Figure 8 were imposed a volume fraction of 25%, the final volume fraction $V_{\text{f,fin}}$ varies considerably. This is mainly due to the maximum size constraint implemented, which is a local constraint that can lead to the optimization being trapped in a local minimum, thus converging to the results shown.

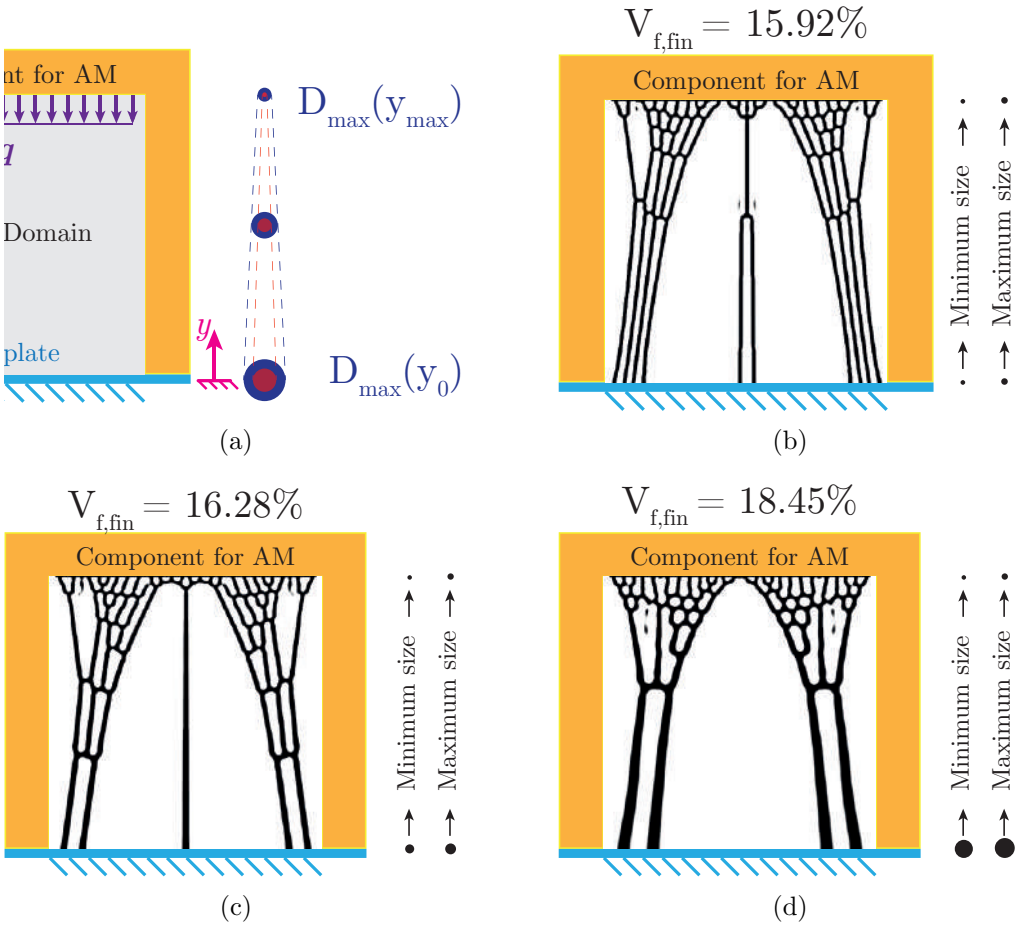

Figure 8: In a) a schematic showing how the minimum and maximum size restrictions linearly decreases. In b) the support generated with a constant maximum size restriction. In c) the support generated with a linear decreases maximum size restriction. In d) support generated with linear decreases maximum size restriction with thicker base length.

To mitigate the discrepancy between the imposed and final volume fractions, one effective approach is to widen the gap between the minimum and maximum sizes of the support structure. This adjustment allows the optimization process more flexibility in varying member thicknesses, as illustrated in Figure 9. This strategy helps to reduce such a difference. Also, the disconnected members, as can be seen in Figure 8, which are a consequence of the maximum size constraint [35], are mitigated. In practice, these small disconnected members do not affect the printability of the support structures, so the presence of this detail is ignored in this work.

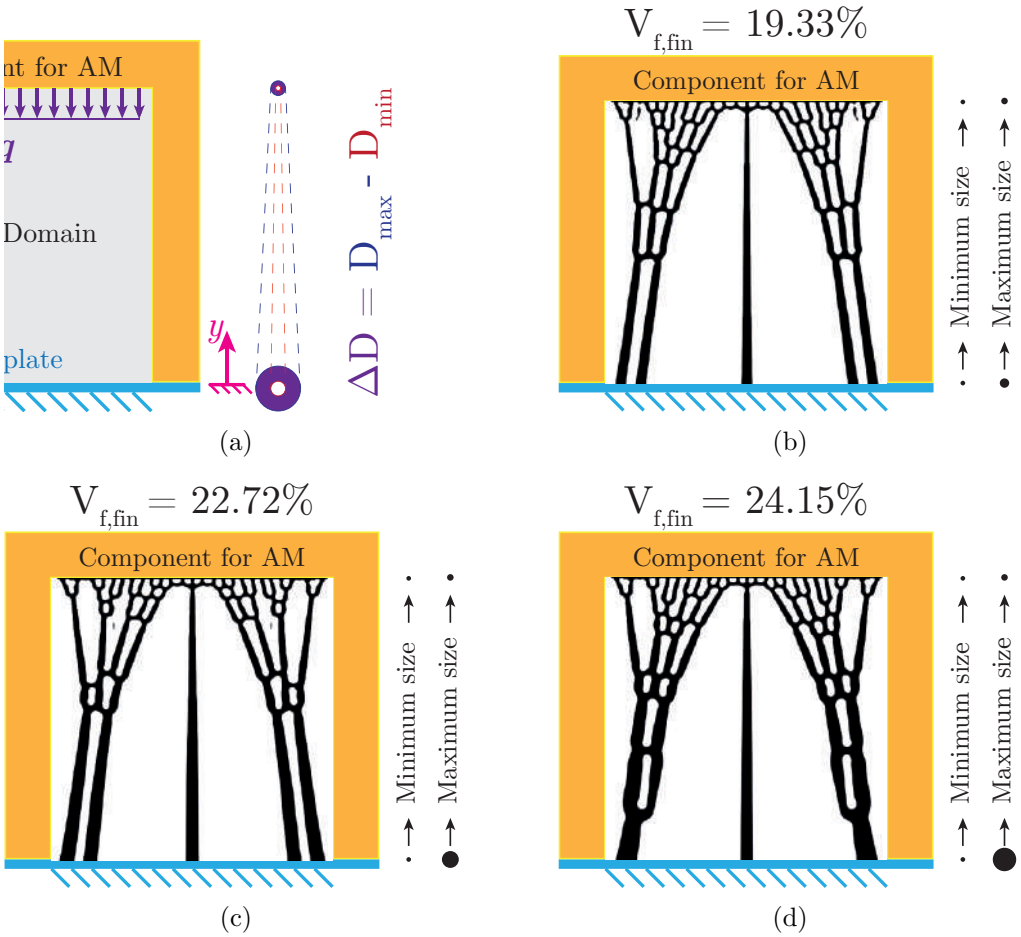

Figure 9: In a) a schematic showing how the spacing between the maximum and minimum size constraint varies. In b) support generated with a distance of 5 elements between the maximum size and minimum size. In c) support generated with a distance of 10 elements between the maximum size and minimum size. In d) support generated with a distance of 15 elements between the maximum size and minimum size.

4.4 Separation between contact points

Finally, to have control over the distance between the contact points of the supports, which is an important property because this distance determines the surface quality of the final part, and, in addition, it can be an important feature considering that many times it is necessary to use tools for the removal of these supports and the space between them must be adequate for the tool to fit. In this work, two strategies are proposed. The first one consists of using the minimum spacing constraint between members that was developed in [25]. This constraint is applied from the base of the support structures, where a spacing of 5 elements is imposed that increases linearly until reaching the desired spacing at the contact points, as can be seen in Figure 10. The second strategy consists of not applying the distributed force that has been conventionally implemented but rather applying separate forces to the elements in which it is desired to have a

contact point, as shown in Figure 11a and whose generated supports are observed in Figure 11.

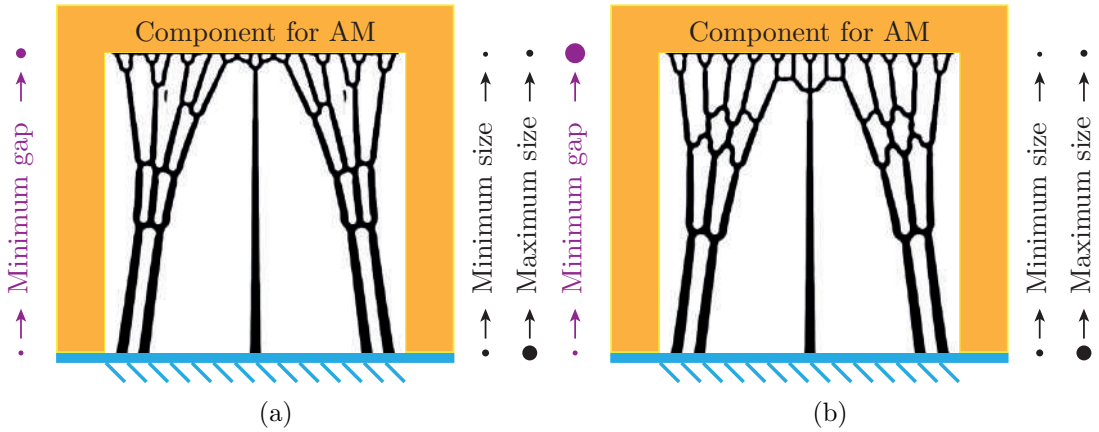

Figure 10: In a) support generated with a minimum separation restriction of 10 element in the contact point. In b) support generated with a minimum size restriction of 20 elements in the contact point.

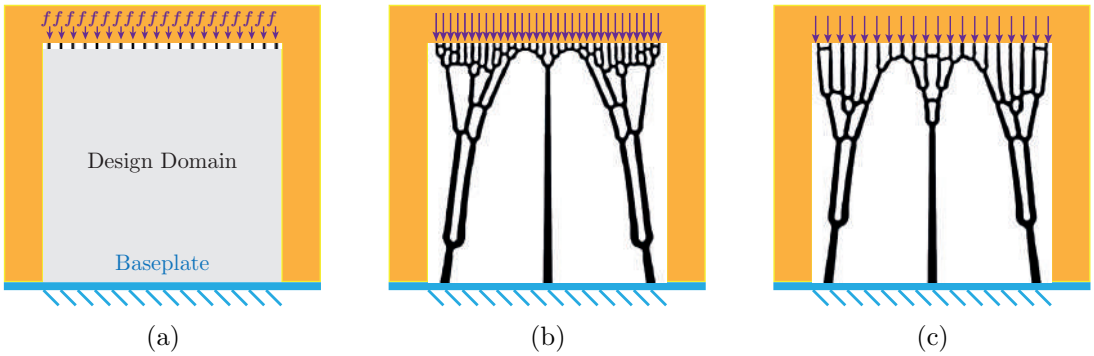

Figure 11: In a) supports generated when separate punctual are applied with a distance of 10 elements. In b) supports generated when punctual forces are applied with a distance of 20 elements.

4.5 Internal supports

In some cases, the support structures cannot be generated from the baseplate of the 3D printer and must be generated from the same piece to be printed. This can become a problem because it not only increases the contact points but also because the supports have large thicknesses at their base. To solve this problem, a maximum size restriction can be imposed at the base of the support structures or in each area where there is a contact point with the part to be printed. Figure 12 shows how this strategy is implemented in a rectangular bridge whose supports cannot be generated from the base. In this, a maximum size constraint is implemented at the base, increasing in size until 25% of the height is reached, then a maximum size constraint is maintained until 65% of the height is reached, and then the maximum size of the supports is decreased again

as they approach the point of contact. The supports generated using this strategy in both the supports generated using a distributed force and a separate forces strategy are shown in Figures 13a and 13b, respectively.

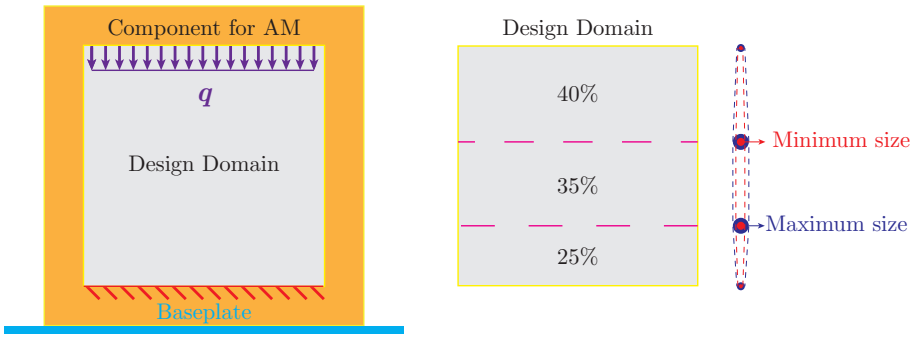

Figure 12: Finite element model used to generate internal supports (left) and the minimum and maximum size imposed through the design domain (right).

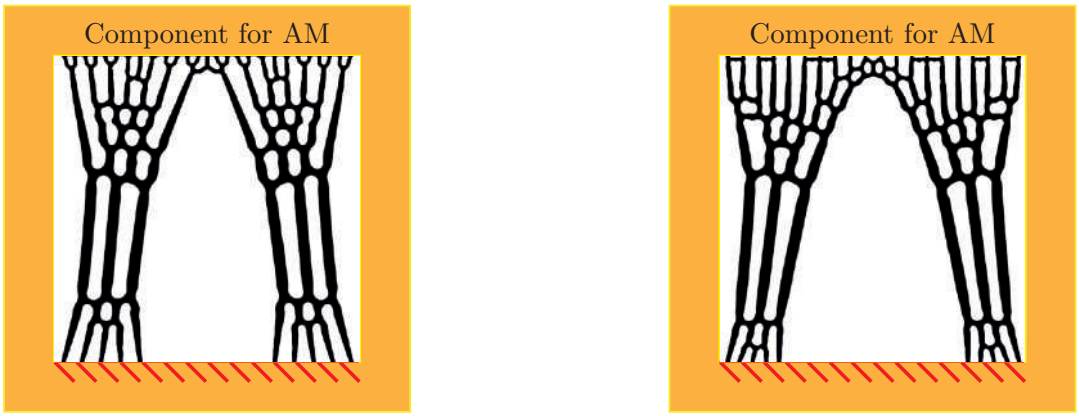

(a) (b)

Figure 13: In a) internal supports generated using a minimum gap constraint. In b) supports generated when punctual forces are applied.

5 NUMERICAL EXAMPLES

To validate our proposed method, we present and analyze the results when applying the strategies to generate support structures with TO for 4 benchmarks, which are shown in Figure 14, and a benchmark whose geometry is more complex as it is the shape of a dog that is observed in Figure 15, where 5 zones are distinguished corresponding to the design spaces of the support structures, which are generated separately and then coupled to the original design. Table 3 shows the minimum size imposed on the base ($r_{\text{min,ini}}$) and on the contact point ($r_{\text{min,fin}}$). The same is true with the maximum size constraint imposed ($r_{\text{max,fin}}$ and $r_{\text{max,fin}}$). In addition, the imposed volume fraction (V_{f}) and the one obtained at the end of the optimization ($V_{\text{f,fin}}$) are shown.

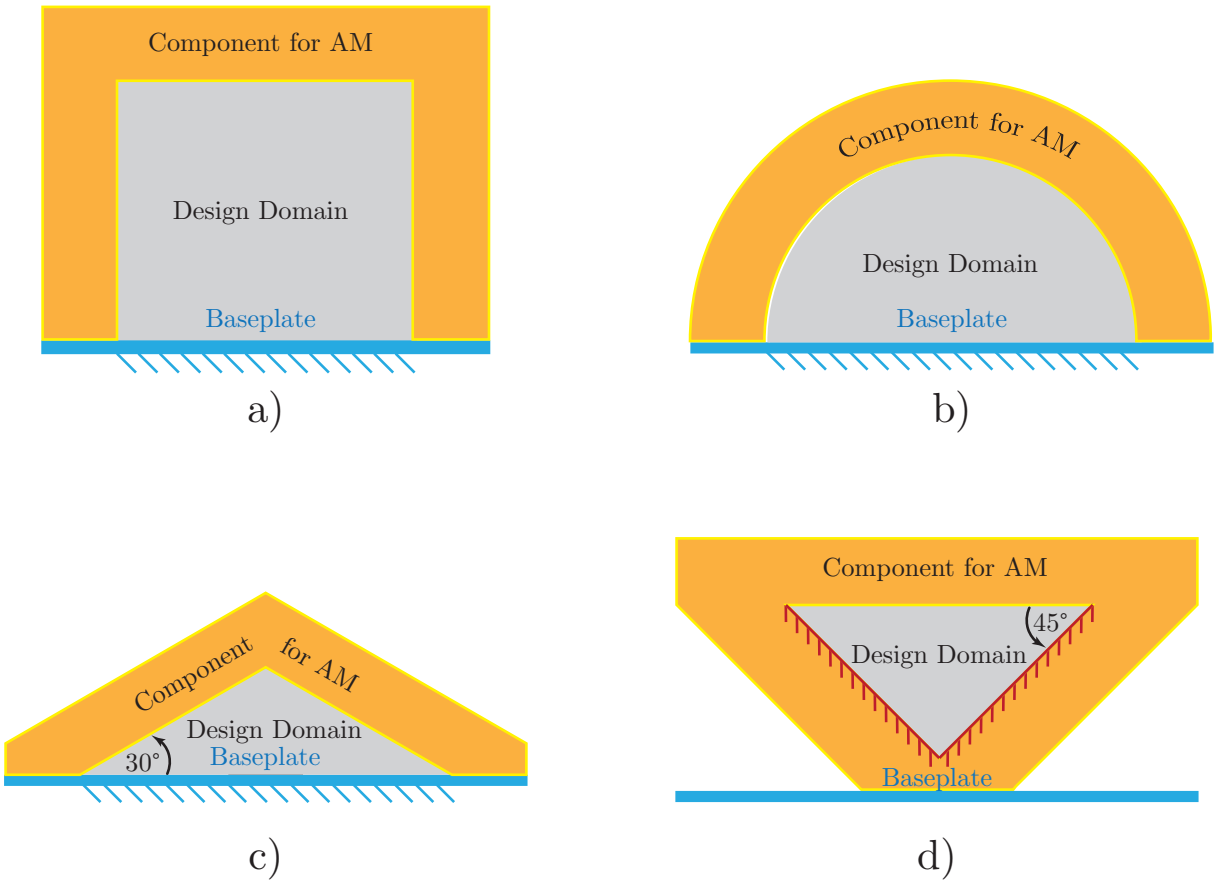

Figure 14: In a) the rectangular bridge. In b) the circular bridge. In c) the triangular bridge. In d) the Inverted triangular bridge.

The support structures generated with TO in MATLAB are matrices of 1 and 0, which are assigned a grayscale color for better visualization. In order to convert these matrices to support structures in a STL format the MATLAB code presented in [36] is used. To create the STL file the "ISO" format is used, intermediate densities greater than 0.5 are rounded to 1 while smaller values are rounded to 0, the extrusion distance of the 2D supports is 5 [mm] which is equal to the thickness of the parts to be supported. These TO-generated supports are attached to the part to be printed using the Meshmixer software [37].

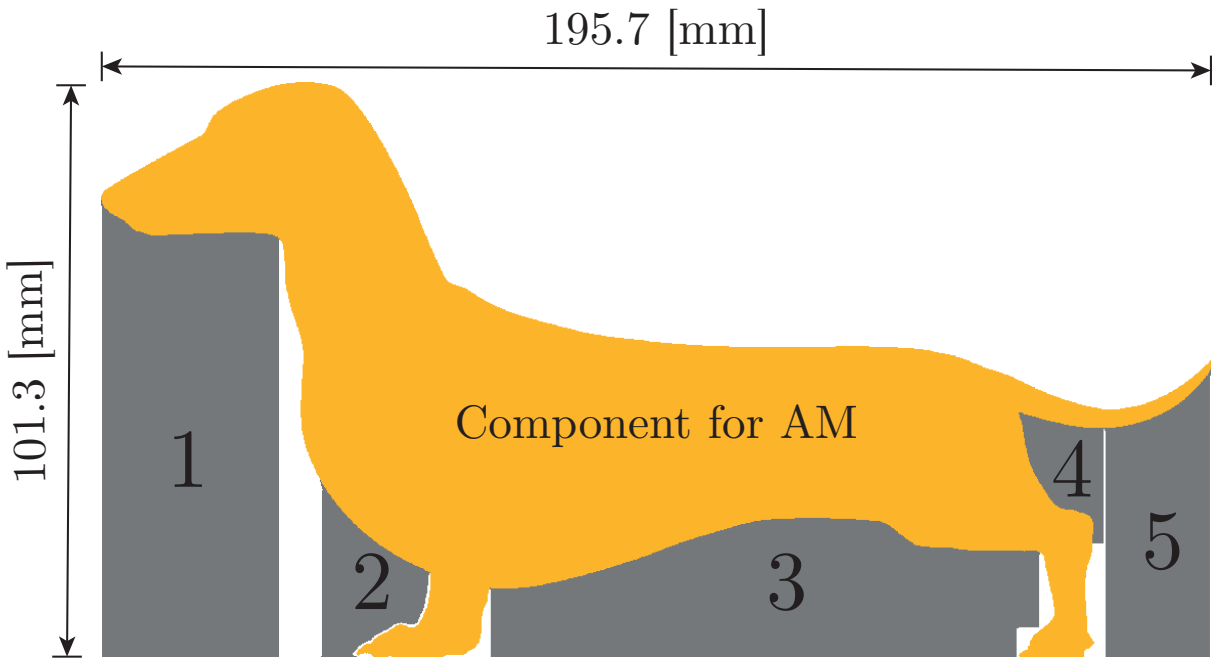

Figure 15: Dog figure used as a benchmark with complex geometry. The gray zones are the design domain used to generate the support structures.

Table 3: Minimum size and maximum size imposed in the support and the volume fraction

Figure	$r_{\text{min,ini}}$	$r_{\text{min,fin}}$	$r_{\text{max,ini}}$	$r_{\text{max,fin}}$	V_{f}	$V_{\text{f,fin}}$
16b	5	2.5	7.5	3.6	30%	20.7%
16c	5	2.5	7.5	3.6	25%	19.1%
17b	5	2.5	7.5	3.6	20%	14.0%
17c	5	2.5	7.5	3.6	20%	16.2%
17d	5	2.5	7.5	3.6	20%	12.9%
18b	4	2.5	6	3.6	20%	18.6%
18c	4	2.5	6	3.6	20%	19.1%
18d	4	2.5	6	3.6	20%	14.5%
19b	5	2.5	7.5	3.6	20%	15.3%
19c	5	2.5	7.5	3.6	20%	17.3%

5.1 Rectangular bridge

The rectangular bridge is mainly characterized by the fact that the distance between the baseplate and the overhanging surface is kept constant. The design space is shown in Figure 16a while Figures 16b and 16c show the supports obtained with TO using a distributed force and applied forces with a distance between them, respectively, and Figures 16d and 16e show the printed parts.

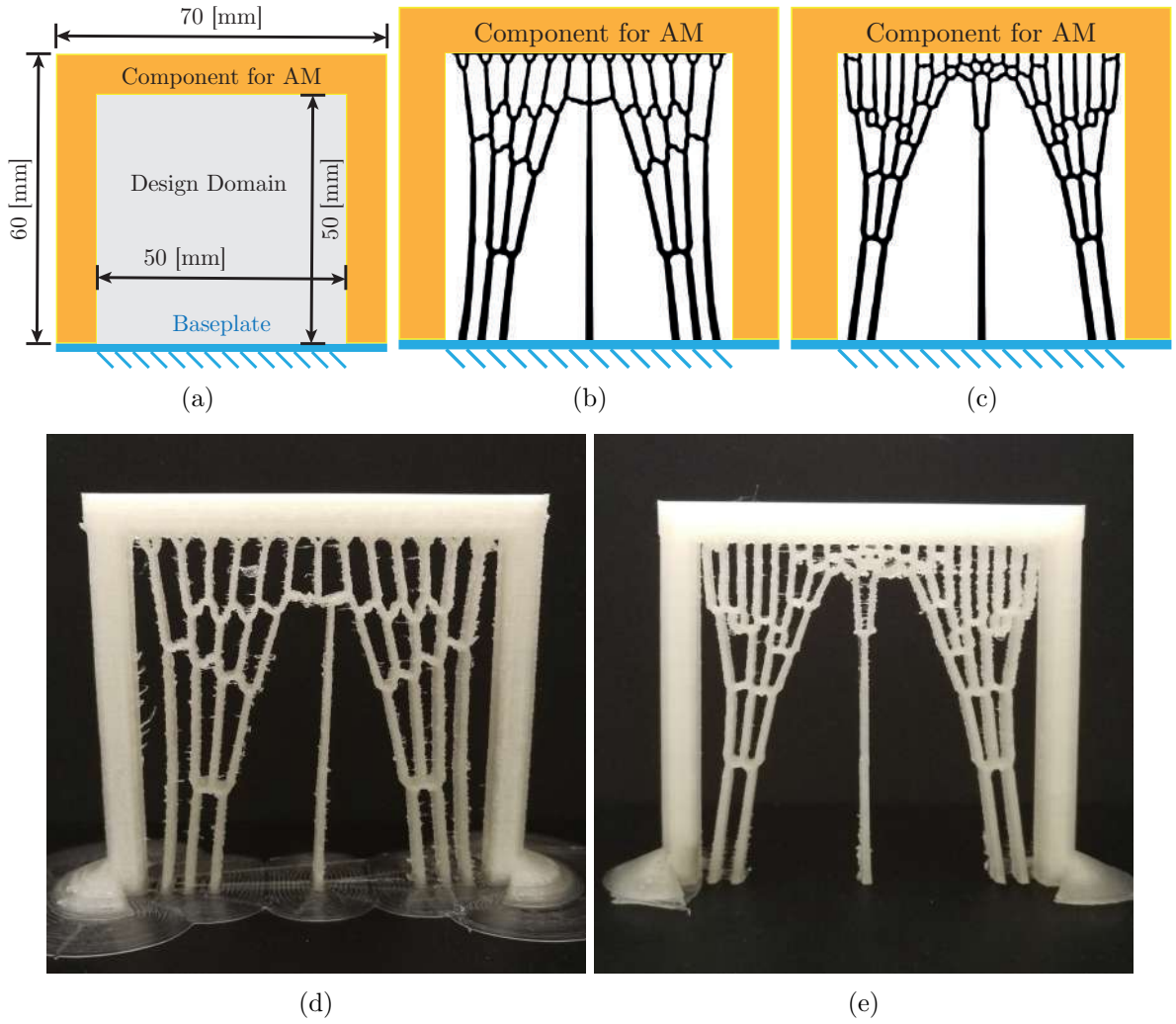

Figure 16: In a) design domain of the rectangular bridge. In b) supports generated with minimum gap restriction. In c) supports generated when separate forces are applied. In d) and e) the printed supports.

5.2 Circular bridge

The circular bridge has the characteristic that part of its structure does not need supports because the angle of inclination is high. Through tests, we determined that structures with angles less than 50^o do not need supports, so the forces in the finite element formulation are only applied to the nodes of the overhang part that have an angle of inclination less than 50^o. Also, it must be considered that the distance between the baseplate of the printer and the overhang surface is not constant. For this reason, modifications are made so that the thickness of the supports at the base decreases as it moves away from the center, thus maintaining the minimum contact area on the top surface. Figure 17a shows the design space, while Figures 17b and 17c show the generated supports. As can be seen in the supports in Figure 17b, in which a distributed force is applied, a roof is formed on the supports that come into contact

with the part to be fabricated. This is a problem since it greatly increases the contact area, making its subsequent removal difficult. To solve this problem, post-processing can be applied to the generated supports to remove this roof manually, finally obtaining the supports shown in Figure 17d. Finally, the supports in Figures 17c and 17d are printed, and the results are shown in Figures 17e and 17f, respectively.

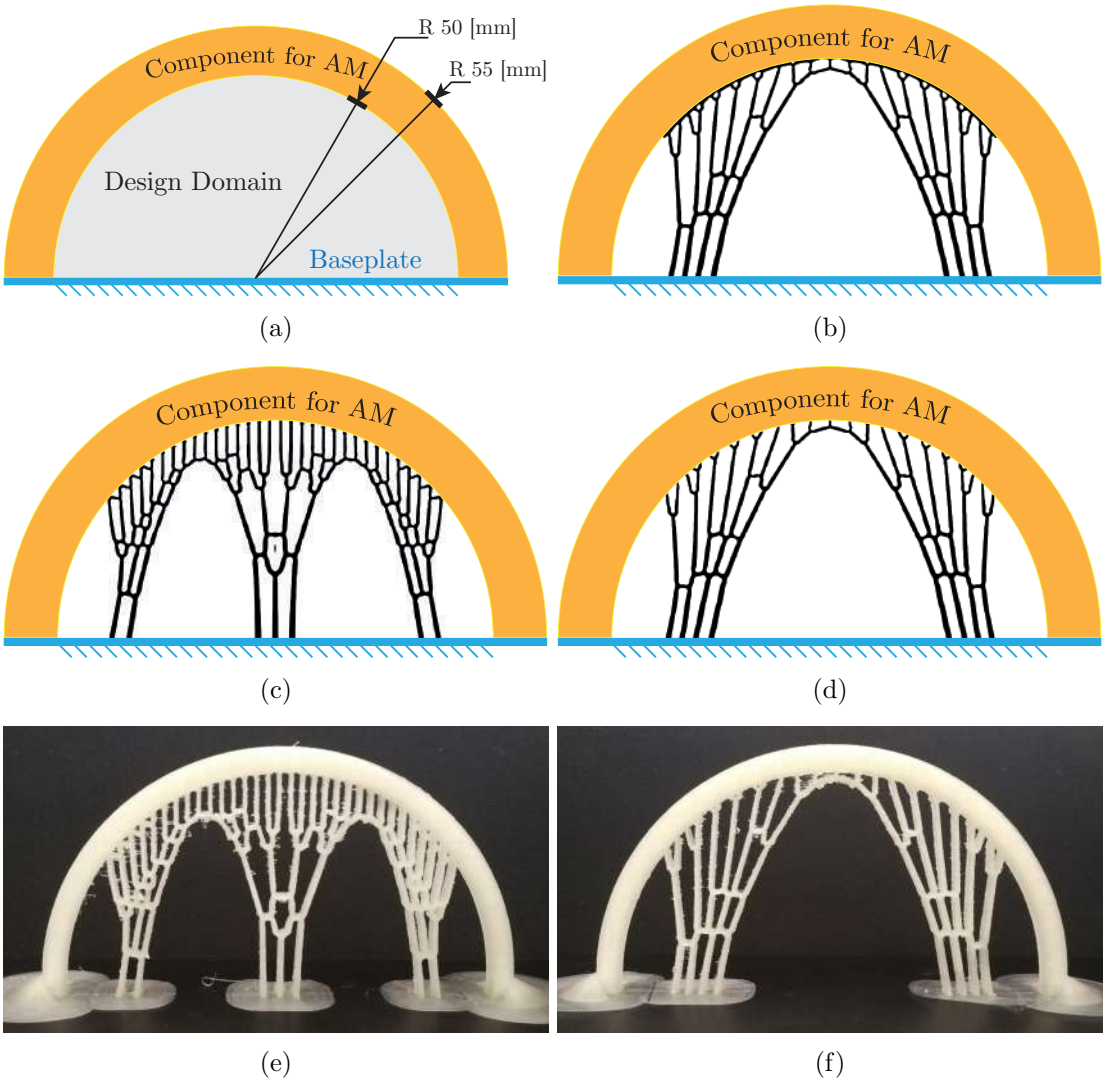

Figure 17: In a) design domain of the circular bridge. In b) supports generated with minimum gap restriction. In c) supports generated when separate forces are applied. In d) supports generated with minimum gap restriction after a post-processing. In e) and f) the printed supports.

5.3 Triangular bridge

As in the previous case, the distance between the overhang surface and the base of the printer increases as it approaches the center, with the difference that this distance varies linearly. As

in the previous case, using the minimum clearance constraint forms a ceiling on the supports, which must be removed with post-processing. Figures 18c and 18d show the supports generated by using point forces and distributed forces, respectively. While Figures 18e and 18f show the printed support structures.

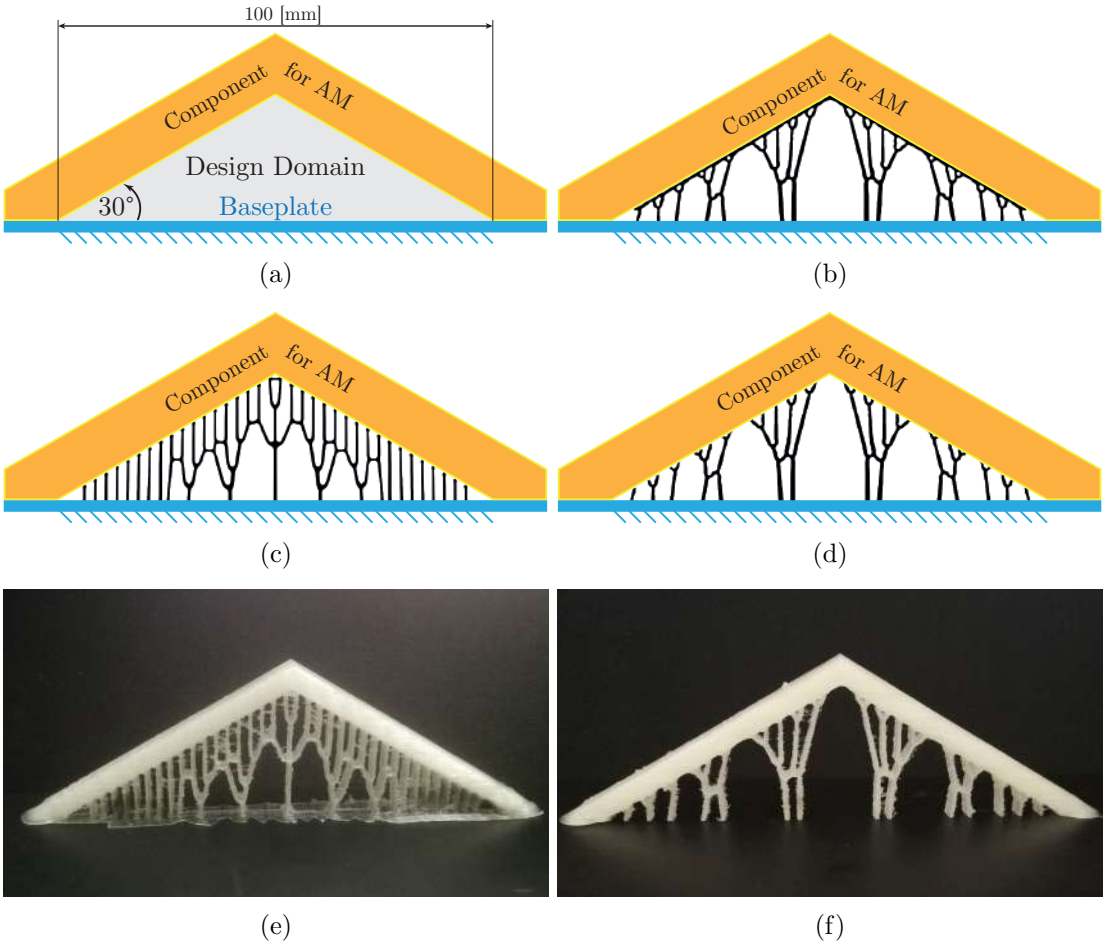

Figure 18: In a) design domain of the triangular bridge. In b) supports generated with minimum gap restriction. In c) supports generated when separate forces are applied. In d) supports generated with minimum gap restriction after a post-processing. In e) and f) the printed supports.

5.4 Inverted triangular bridge

Unlike the previous cases, this one has the particularity that the supports are generated in the same piece to be printed and not from the baseplate of the printer. Therefore, it is necessary not to use large thicknesses in the base of the support structures so as not to hinder subsequent removal. Figure 19a shows the design space, while Figures 19b and 19c show the generated supports. The printed supports can be seen in Figures 19e and 19d.

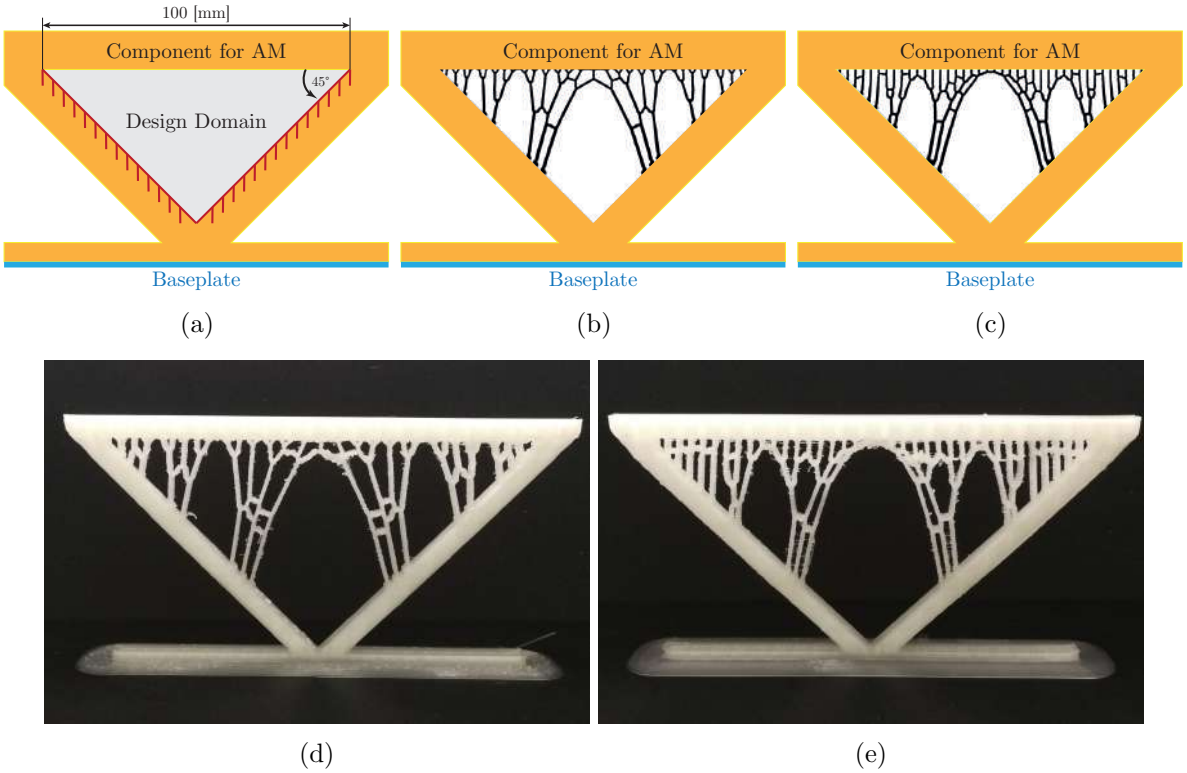

Figure 19: In a) design domain of the inverted triangular bridge. In b) supports generated with minimum gap restriction. In c) supports generated when separate forces are applied. In d) and e) the printed supports.

Finally, we compared the efficiency of the supports for each of the representative geometries with the supports generated by the Cura software. The results are obtained by the same software and shown in Table 4. In this table, only the supports generated using punctual forces are compared because this is the method that best controls the distance between the contact points. It is worth mentioning that only the efficiency of the supports is compared, not their effectiveness to achieve good surface quality or to avoid possible deformations. In that case, it would be interesting to use the benchmarks proposed in [38]. It can be observed that the supports generated with TO are more efficient than those generated by the Cura software and, in some cases, require less printing time.

5.5 Complex geometry

Finally, the supports generated with TO are used for a case whose geometry is more complex. Figure 20a shows supports generated using a distributed force, and Figure 20b shows supports generated using point forces. The printed supports can be seen in Figures 20c and 20d, respectively.

Table 4: Numerical comparison of support structures computed by TO and by Cura software.

Component	Total mass	Print time	Mass reduction with TO
Rectangular bridge (Cura)	8 g	6 h 45 min	-
Rectangular bridge (TO)	7 g	6 h 26 min	12.5 (%)
Circular bridge (Cura)	9 g	7 h 43 min	-
Circular bridge (TO)	8 g	7 h 45 min	11.1 (%)
Triangular bridge (Cura)	6 g	4 h 32 min	-
Triangular bridge (TO)	5 g	4 h 57 min	16.7 (%)
Inv. triangular bridge (Cura)	11 g	8 h 25 min	-
Inv. triangular bridge (TO)	9 g	7 h 28 min	18.2 (%)

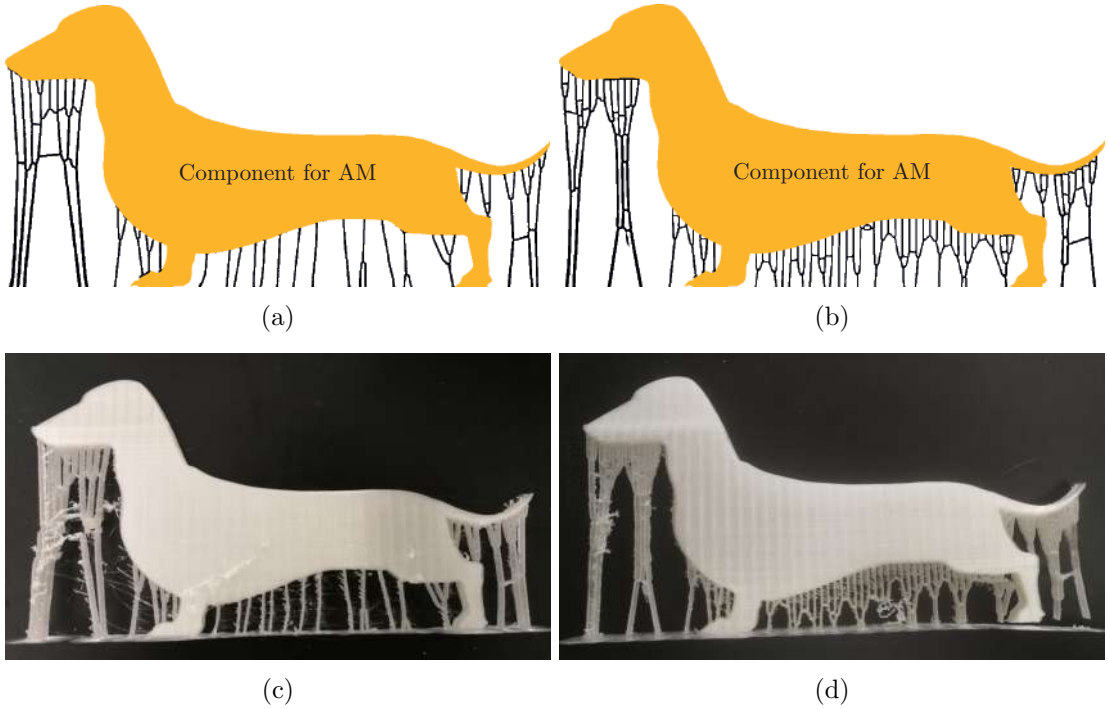

Figure 20: In a) supports generated with a minimum gap restriction. In b) supports generated when separate forces are applied. In c) and d) the printed supports.

The results obtained by using a distributed force with a minimum gap constraint meet the requirement of having small contact areas and supporting the structure to be printed. However, it is not precise when controlling the minimum distance, and in some cases, it is necessary to apply post-processing to obtain good results. On the other hand, by using point forces, small contact areas can be obtained without the need for post-processing, and the distance between the contact points can be precisely controlled. Moreover, since it is not necessary to implement a minimum gap constraint between members, the strategy is much less computationally expensive than using a distributed force.

6 CONCLUSION

This work has explored the use of TO for designing support structures for AM. Specifically, a density-based TO formulation with minimum and maximum size control has been adopted. To ensure good 3D printability, the geometric control in TO was imposed according to a set of geometric guidelines collected for an Ultimaker S2$^+$ printer, and two strategies to control the space between the contact points were analyzed. The proposed methodology and the contributions of this work lead to the following conclusions:

- Current TO methods allow for taking into account several geometric constraints associated with 3D printing. In this work, the minimum wall thickness, minimum separation between walls, minimum cavity size, maximum bridge span, and maximum aspect ratio were considered.
- The maximum aspect ratio can be implicitly imposed in TO by defining the minimum member size in terms of the layer height.
- The maximum size restrictions promote structural redundancy, which increases the amount of branching in the support structures. This could stiffen the support, especially in directions orthogonal to the building direction.
- The use of punctual forces spaced according to the geometric guidelines reduces the contact zones between the support and the AM component, which facilitates their removal.

The work was developed using 2D design domains, which were extruded for experimental validation. Future efforts will be put into the 3D validation of the proposed methodology.

REFERENCES

[1] Mary Kathryn Thompson, Giovanni Moroni, Tom Vaneker, Georges Fadel, R Ian Campbell, Ian Gibson, Alain Bernard, Joachim Schulz, Patricia Graf, Bhrigu Ahuja, et al. Design for additive manufacturing: Trends, opportunities, considerations, and constraints. *CIRP annals*, 65(2):737–760, 2016.

[2] Jacopo Lettori, Roberto Raffaeli, Margherita Peruzzini, Juliana Schmidt, and Marcello Pellicciari. Additive manufacturing adoption in product design: an overview from literature and industry. *Procedia Manufacturing*, 51:655–662, 2020.

[3] Jihong Zhu, Han Zhou, Chuang Wang, Lu Zhou, Shangqin Yuan, and Weihong Zhang. A review of topology optimization for additive manufacturing: status and challenges. *Chinese Journal of Aeronautics*, 2020.

[4] Antonio Armillotta, Mattia Bellotti, and Marco Cavallaro. Warpage of fdm parts: Experimental tests and analytic model. *Robotics and Computer-Integrated Manufacturing*, 50:140–152, 2018.

[5] Paul Alexander, Seth Allen, and Debasish Dutta. Part orientation and build cost determination in layered manufacturing. *Computer-Aided Design*, 30(5):343–356, 1998.

[6] Paramita Das, Kunal Mhapsekar, Sushmit Chowdhury, Rutuja Samant, and Sam Anand. Selection of build orientation for optimal support structures and minimum part errors in additive manufacturing. *Computer-Aided Design and Applications*, 14(sup1):1–13, 2017.

[7] Kailun Hu, Shuo Jin, and Charlie CL Wang. Support slimming for single material based additive manufacturing. *Computer-Aided Design*, 65:1–10, 2015.

[8] Emiel van de Ven, Robert Maas, Can Ayas, Matthijs Langelaar, and Fred van Keulen. Overhang control based on front propagation in 3d topology optimization for additive manufacturing. *Computer Methods in Applied Mechanics and Engineering*, 369:113169, 2020.

[9] Lin Cheng, Xuan Liang, Jiaxi Bai, Qian Chen, John Lemon, and Albert To. On utilizing topology optimization to design support structure to prevent residual stress induced build failure in laser powder bed metal additive manufacturing. *Additive Manufacturing*, 27:290–304, 2019.

[10] Jingchao Jiang, Xun Xu, and Jonathan Stringer. Support structures for additive manufacturing: a review. *Journal of Manufacturing and Materials Processing*, 2(4):64, 2018.

[11] Paul Didier, Gael Le Coz, Guillaume Robin, Paul Lohmuller, Boris Piotrowski, Abdelhadi Moufki, and Pascal Laheurte. Consideration of slm additive manufacturing supports on the stability of flexible structures in finish milling. *Journal of Manufacturing Processes*, 62:213–220, 2021.

[12] Giorgio Strano, L Hao, RM Everson, and KE Evans. A new approach to the design and optimisation of support structures in additive manufacturing. *The International Journal of Advanced Manufacturing Technology*, 66(9-12):1247–1254, 2013.

[13] Ahmed Hussein, Liang Hao, Chunze Yan, Richard Everson, and Philippe Young. Advanced lattice support structures for metal additive manufacturing. *Journal of Materials Processing Technology*, 213(7):1019–1026, 2013.

[14] Lin Lu, Andrei Sharf, Haisen Zhao, Yuan Wei, Qingnan Fan, Xuelin Chen, Yann Savoye, Changhe Tu, Daniel Cohen-Or, and Baoquan Chen. Build-to-last: Strength to weight 3d printed objects. *ACM Transactions on Graphics (TOG)*, 33(4):1–10, 2014.

[15] Juraj Vanek, Jorge A Garcia Galicia, and Bedrich Benes. Clever support: Efficient support structure generation for digital fabrication. In *Computer graphics forum*, volume 33, pages 117–125. Wiley Online Library, 2014.

[16] Ruiliang Feng, Xianda Li, Lin Zhu, Atul Thakur, and Xiangzhi Wei. An improved two-level support structure for extrusion-based additive manufacturing. *Robotics and Computer-Integrated Manufacturing*, 67:101972, 2021.

[17] Martin Philip Bendsøe and Noboru Kikuchi. Generating optimal topologies in structural design using a homogenization method. *Computer methods in applied mechanics and engineering*, 71(2):197–224, 1988.

[18] Grégoire Allaire and Beniamin Bogosel. Optimizing supports for additive manufacturing. *Structural and Multidisciplinary Optimization*, 58(6):2493–2515, 2018.

[19] Oliver Giraldo-Londoño, Lucia Mirabella, Livio Dalloro, and Glaucio H Paulino. Multi-material thermomechanical topology optimization with applications to additive manufacturing: Design of main composite part and its support structure. *Computer Methods in Applied Mechanics and Engineering*, 363:112812, 2020.

[20] Takao Miki and Shinji Nishiwaki. Topology optimization of the support structure for heat dissipation in additive manufacturing. *arXiv preprint arXiv:2108.01815*, 2021.

[21] Yu-Hsin Kuo, Chih-Chun Cheng, Yang-Shan Lin, and Cheng-Hung San. Support structure design in additive manufacturing based on topology optimization. *Structural and Multidisciplinary Optimization*, 57(1):183–195, 2018.

[22] Matthijs Langelaar. Combined optimization of part topology, support structure layout and build orientation for additive manufacturing. *Structural and Multidisciplinary Optimization*, 57(5):1985–2004, 2018.

[23] Francesco Mezzadri, Vladimir Bouriakov, and Xiaoping Qian. Topology optimization of self-supporting support structures for additive manufacturing. *Additive Manufacturing*, 21:666–682, 2018.

[24] Ultimaker. Ultimaker Cura: software de impresión 3D potente y fácil de usar | Ultimaker, 2020.

[25] Eduardo Fernández, Kai-ke Yang, Stijn Koppen, Pablo Alarcón, Simon Bauduin, and Pierre Duysinx. Imposing minimum and maximum member size, minimum cavity size, and minimum separation distance between solid members in topology optimization. *Computer Methods in Applied Mechanics and Engineering*, 368:113157, 2020.

[26] Ole Sigmund and Joakim Petersson. Numerical instabilities in topology optimization: a survey on procedures dealing with checkerboards, mesh-dependencies and local minima. *Structural optimization*, 16(1):68–75, 1998.

[27] Fengwen Wang, Boyan Stefanov Lazarov, and Ole Sigmund. On projection methods, convergence and robust formulations in topology optimization. *Structural and Multidisciplinary Optimization*, 43(6):767–784, 2011.

[28] Tyler E Bruns and Daniel A Tortorelli. Topology optimization of non-linear elastic structures and compliant mechanisms. *Computer methods in applied mechanics and engineering*, 190(26-27):3443–3459, 2001.

[29] Ole Sigmund. Manufacturing tolerant topology optimization. *Acta Mechanica Sinica*, 25(2):227–239, 2009.

[30] Jingchao Jiang, Jonathan Stringer, Xun Xu, and Ray Y Zhong. Investigation of printable threshold overhang angle in extrusion-based additive manufacturing for reducing support waste. *International Journal of Computer Integrated Manufacturing*, 31(10):961–969, 2018.

[31] Eustaquio García Plaza, Pedro José Núñez López, Miguel Ángel Caminero Torija, and Jesús Miguel Chacón Muñoz. Analysis of pla geometric properties processed by fff additive manufacturing: Effects of process parameters and plate-extruder precision motion. *Polymers*, 11(10):1581, 2019.

[32] Omar A Mohamed, Syed H Masood, and Jahar L Bhowmik. Optimization of fused deposition modeling process parameters: a review of current research and future prospects. *Advances in Manufacturing*, 3(1):42–53, 2015.

[33] Mani Mahesh, YS Wong, JYH Fuh, and HT Loh. Benchmarking for comparative evaluation of rp systems and processes. *Rapid Prototyping Journal*, 2004.

[34] Amit J Lopes, Mireya A Perez, David Espalin, and Ryan B Wicker. Comparison of ranking models to evaluate desktop 3d printers in a growing market. *Additive Manufacturing*, 35:101291, 2020.

[35] Eduardo Fernández, Maxime Collet, Pablo Alarcón, Simon Bauduin, and Pierre Duysinx. An aggregation strategy of maximum size constraints in density-based topology optimization. *Structural and Multidisciplinary Optimization*, 60(5):2113–2130, 2019.

[36] Kai Liu. Top3dSTL_v3, 2021.

[37] Autodesk. Meshmixer, 2021.

[38] Jonathan Stringer, Xun Xu, Pai Zheng, and Jingchao Jiang. A benchmarking part for evaluating and comparing support structures of additive manufacturing. In *International Conference on Progress in Additive Manufacturing (Pro-AM 2018)*, volume 196, page 201, 2018.